Heliyon 10 (2024) e37511

Contents lists available at ScienceDirect

Heliyon

journal homepage: www.cell.com/heliyon

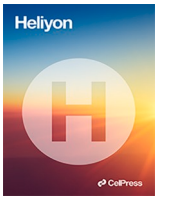

Research article

Single-cell RNA sequencing analysis reveals the distinct features of colorectal cancer with or without *Fusobacterium nucleatum* infection in PD-L1 blockade therapy

Tingting Ding [a,e,1], Qian Chen [b,1], Hu Liu [a,1], Heping Zhang [c], Yuefang Sun [a], Lamei Zhao [d], Yaohui Gao [a,*], Qing Wei [a,**]

[a] *Department of Pathology, Shanghai Tenth People's Hospital, Tongji University School of Medicine, Shanghai, 200072, China*
[b] *Research Institute of Intestinal Diseases, Shanghai Tenth People's Hospital, Tongji University School of Medicine, Shanghai, China*
[c] *Department of Oncology, Shanghai Tenth People's Hospital, Tongji University School of Medicine, Shanghai, 200072, China*
[d] *Department of Pathology, Shanghai Clinical College, Anhui Medical University, Hefei, Anhui, China*
[e] *Department of Medical Oncology, Jinling Hospital, Affiliated Hospital of Medicine School, Nanjing University, Nanjing, China*

ARTICLE INFO

Keywords:
Colorectal cancer
Single-cell RNA sequencing
PD-L1 blockade
Fusobacterium nucleatum
Immunotherapy

ABSTRACT

MSS/pMMR patients are unresponsive to PD-1/PD-L1 blockade in colorectal cancer (CRC), but the mechanisms are unclear. A better understanding of immunotherapy resistance in CRC may lead to more precise treatment and expand the benefit of immunotherapy to patients. In this study, we constructed mouse model of subcutaneous CRC tumor received anti-PD-L1 treatment with or without *fusobacterium nucleatum* (*F. nucleatum*) infection. Then we used single-cell RNA sequencing (scRNA-seq) to explore the comprehensive landscape of the tumor microenvironment (TME). Our data delineated the composition, subclonal diversity and putative function of distinct cells, tracked the developmental trajectory of tumor cells and highlighted cell-cell interactions. We found different compositions and functions of both tumor cells and immune cells. Single anti-PD-L1 monoclonal antibody (mAb) treated tumor exhibited two specific clusters which might be resistant to PD-L1 blockade. The accumulation of immune cells, including T cell, NK cell and pro-inflammatory macrophage subset in tumors infected with *F. nucleatum* may be one of the reasons for the increased sensitivity to PD-L1 blockade. Thus, targeting *F. nucleatum* to change the composition of tumor cell subclusters and enliven the immune response might help to overcome immune checkpoint blockade (ICB) resistance.

1. Introduction

Though standard conventional treatments have made substantial progress, colorecatal cancer (CRC) ranked third of newly diagnosed cases and second of cancer-related deaths [1]. Owing to the burden of CRC incidence and mortality, efforts to perform in-depth insight into its pathogenesis, development and treatments are critical. CRC originates from complex and heterogeneous etiological factors and pathogenetic mechanisms. Chromosomal instability, microsatellite instability (MSI) and the CpG island methylation

* Corresponding author. No. 301, Yanchang Middle Road, Jing'an District, Shanghai China.
** Corresponding author. No. 301, Yanchang Middle Road, Jing'an District, Shanghai, China.
E-mail addresses: gaoyaohui187@tongji.edu.cn (Y. Gao), weiqing1971@126.com (Q. Wei).
[1] These authors contributed equally to this work.

https://doi.org/10.1016/j.heliyon.2024.e37511
Received 11 October 2023; Received in revised form 28 August 2024; Accepted 4 September 2024
Available online 6 September 2024

pathway (CIMP) are three major molecular pathways causing CRC. Among the process of carcinogenesis, gut microbes play a role in the conversion of healthy intestinal to dysplastic [2]. *Fusobacterium nucleatum* (*F. nucleatum*), an anaerobic bacterium enriched in intestinal tissues, is associated with initiating and promoting colorectal carcinogenesis [3–5]. A better understanding of the relationship between *F. nucleatum* and tumor microenvironment (TME) may provide new targets for CRC prevention and therapy.

In recent years, due to the increasing knowledge in tumor development, novel anti-tumor treatments are constantly emerging [6–9]. Among these therapies, immune checkpoint blockade (ICB), especially anti-PD-1 and anti-PD-L1 mAb, has revolutionized cancer therapy as an effective and durably responsive approach in various cancers, including melanoma, non-small cell lung cancer (NSCLC), liver cancer, and CRC [10–12]. The patients characterized by high tumor mutation burden, positive PD-L1 expression, MSI phenotype and enriched lymphocyte infiltration are more sensitive to ICB [13–16]. However, a proportion of these with initial response eventually relapse during the treatment [17]. In this scenario, it is essential to understand the mechanisms of immunotherapy resistance. It has been suggested that lack of PD-L1 expression, loss of neoantigen, T Cell exclusion, immune dysfunction, metabolism and epigenetics are associated with poor response to anti-PD therapy in tumors. One approach to overcoming PD-L1 mAb resistance is combination with other drug targets, for example chemotherapy, radiotherapy, anti-VEGF targeted therapies and other immunotherapy, such as anti-CTLA-4 therapy [18]. Of note, a relationship was found between microbiota diversity and improved immunotherapy efficiency, even including some pathogenic bacteria, such as *F. nucleatum* and *enterotoxigenic Bacteroides fragilis* [19,20]. Our previous study has shown that *F. nucleatum* enhances the sensitivity of CRC to anti-PD-L1 therapy, but the mechanism remains elusive and need further investigations [20].

In this study, we performed single-cell RNA sequencing (scRNA-seq) to compare the gene expression pattern and associated pathways of each individual cell between anti-PD-L1 treated CRC samples with or without *F. nucleatum* infection. We then tracked the developmental trajectory of tumor cells to uncover their differentiation direction influenced by distinct stimuli in the TME. Finally, we analyzed the intercellular signaling networks between diverse cells. Based on the results, we can better understand the distinct features of CRC that are sensitive or insensitive to PD-L1 blockade and unmasked how *F. nucleatum* regulated the TME.

2. Material and methods

2.1. Sample collection and preparation of single-cell suspensions

Xenograft experiments were performed according to our previous study [20]. Briefly, 4–6 weeks BALB/c mice were fed with drinking water with Streptomycin (2 mg/ml) and penicillin (2000 U/ml) for 1 week before CT26.WT cell (5×10^5, purchased from ATCC, CRL-2638) were subcutaneously injected into the right armpit of the mice. Once the subcutaneous tumor reached 100 m^3, mice received an intraperitoneal injection of an anti-PD-L1 mAb (αPD-L1, BP0101, BioXcell) or an isotype control mAb, combined with an intratumoral injection of *F. nucleatum*, or phosphate-buffered saline (PBS) every 3 days. Tumor samples were grouped as the control tumor (isotype control mAb with PBS), the αPD-L1 tumor (αPD-L1 with PBS), the *Fn* tumor (isotype control mAb with *F. nucleatum*) and the *Fn*+αPD-L1 tumor (αPD-L1 with *F. nucleatum*), respectively. Once the mice were sacrificed, the subcutaneous tumors were collected immediately and minced into small pieces after washed three times with Hanks' balanced salt solution (Sigma-Aldrich). Then we digested them by incomplete Roswell Park Memorial Institute 1640 with endotoxin free collagenase I (2 mg/mL; Sigma-Aldrich) for 1 h at 37 °C, followed by filtering impurities with a 45 μm sterile strainer. The single-cell suspensions were resuspended at a concentration of 1000 cells/milliliter (mL). 5 mL of erythrocyte lysis solution was added to the cell suspension for 5 min. Animal experiments were conducted in accordance with the National Institutes of Health Guidelines for the Care and Use of Laboratory Animals. The study procedures were approved by the Institutional Animal Care and Use Committee of Shanghai Tenth People's Hospital, School of Medicine, Tongji University (ID Number: SHSY-2018–3566).

2.2. ScRNA library construction, sequencing, quality control (QC) and gene quantification

The library construction and sequencing were completed by OE Biotech Co., Ltd. (Shanghai, China) following the User Guide of Chromium Next GEM Single Cell 3′ GEM, Library & Gel Bead Reagent Kits v3.1 (Cat. No. PN-1000121). The 10x genomics official software CellRanger (version 3.1.0) was used to quantify the high-throughput single cell transcriptome by identifying the barcode sequence markers and the Unique Molecular Identifier (UMI) of different mRNA molecules in each cell. Then QC statistics was conducted on the raw sequencing data which were aligned to the mouse reference genome.

2.3. Gene quantitative QC and data preprocessing

The Seurat software package (version 3.1.1) was used to further control and process the data. Based on the distribution of the number of expressed gene (nGene), the number of UMI (nUMI), and the percentage of mitochondrial gene expression (percent. mito) in most cells, the generalized linear model was fitted to filter the outlier cells and low-quality cells that with gene and UMI beyond the range of the mean ± 2 times standard deviation and percent. mito more than 20%.

2.4. Dimension reduction and cluster analysis

Principal component analysis was performed on the basis of gene expression, the result of which were visualized in two-dimensional space through t-distributed Stochastic Neighbor Embedding (t-SNE). Mutual nearest neighbor reduction was used to

correct the batch effect of single cell expression profile data. The similarity between two cell clusters was determined by calculating the Pearson correlation coefficient of the mean gene expression.

2.5. Differentially expressed genes (DEGs) and functional analysis

The FindAllMarkers function in the Seurat package was used to identify DEGs with fold change more than 1.5 and p value less than 0.05 by MAST difference test algorithm. The functional annotation and enrichment analysis of Gene Ontology (GO) and Kyoto Encyclopedia of Genes and Genomes (KEGG) were performed using R software based on the hypergeometric distribution. P value was adjusted with the Benjamini–Hochberg method and adjust $p < 0.05$ was considered significant.

2.6. Cell type identification

For cell type identification, we used the R package SingleR with the reference transcriptomic datasets Immunological Genome Project (ImmGen) to infer the cell of origin of each of the single cells independently [21]. Then canonical markers were used to further validate the annotation results as follows: fibroblasts-Sparc, Dcn, Cald1 [22–24]; epithelial cells-Epcam; smooth muscle cell- Smtn; endothelial cell-Pecam1 [25]; T cells-Cd3e, CD4 T cells -Cd4, CD8 T cells-Cd8a, NK cells-Ncr1 [26]; macrophages-Cd14 and Cd68 [27]; neutrophils-Ly6g [28].

2.7. CNV analysis

The CNV level of tumor cells was determined using inferCNV (https://github.com/broadinstitute/inferCNV) by comparing the gene expression density on the genome of tumor cells with infiltrated immune cells as reference control. The relative expression density of genes on each chromosome was visualized through heatmaps which displayed the overexpression and absent expression regions. Residual expression filtering was used to reduce the noise signal in the data so as to discover the true CNV signal.

2.8. Interaction network construction

To investigate intercellular communication networks between different cell types in the four tumor samples, the normalized scRNA-seq data was imported into the R package Cellchat. We performed 'Secreted Signaling', 'ECM-Receptor', and 'Cell-Cell Contact' with a standard parameter set according to the official workflow.

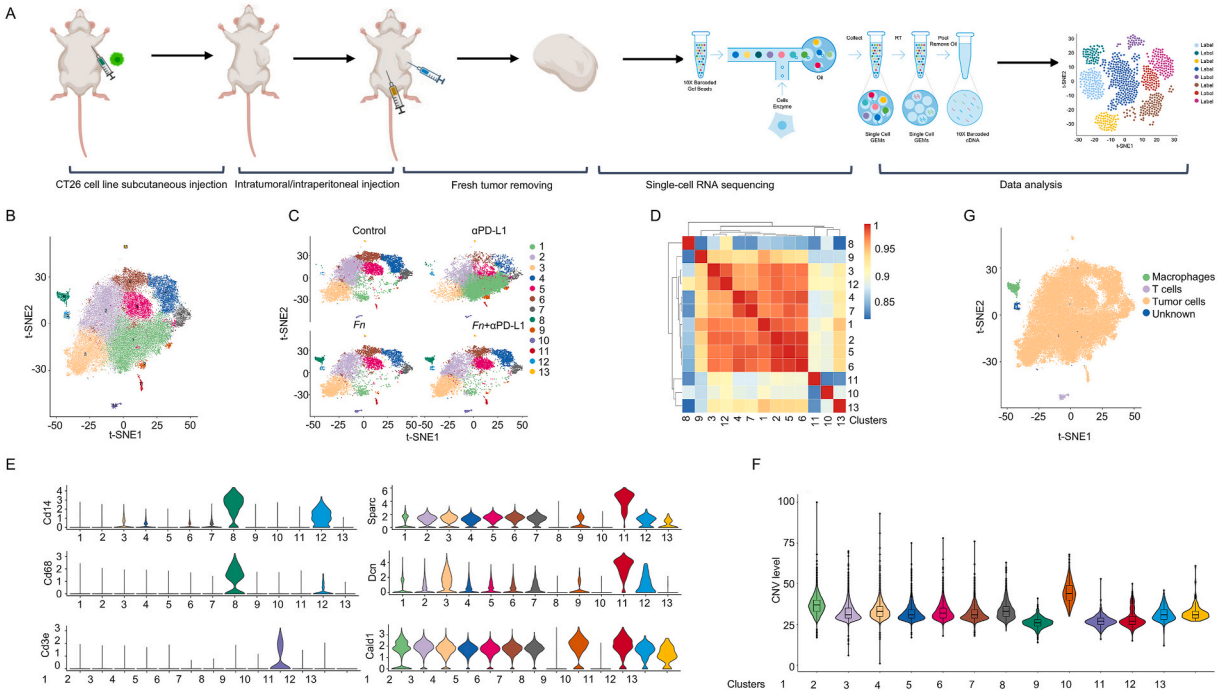

Fig. 1. Cells of the tumor tissues are clustered into 13 subpopulations and are identified to be tumor cells, T cells and macrophages, respectively. (A) Experiment workflow of this study. (B) Cell clustering displayed by t-distributed Stochastic Neighbor Embedding (t-SNE). (C) The compositions of cell clusters in different tumor samples. (D) Heatmap shows the similarity among diverse cell clusters. (E) Canonical markers of common cell types in the tumor microenvironment (TME). (F) Chromosome copy number variation (CNV) values of each cluster. (G) Cell type identification.

2.9. Trajectory analysis

We employed Monocle 2 software package to calculate the expression pattern of key genes. Based on the results, machine learning was used to simulate the dynamic changes during the cellular development process. Then dimension reduction was carried out according to expression profile of largely varied genes between cells. Finally, a minimum spanning tree was built to find the longest trajectory representing the differentiation track of cells with similar transcription characteristics. Cells in the control sample were chosen as the beginning of pseudotime trajectory.

2.10. Calculation of macrophage inflammatory and polarization scores

Genes characterizing macrophages, including pro-inflammatory and anti-inflammatory genes, as well as M1 and M2 phenotype related genes were selected from previous literature (Table S1) [29]. Seurat's AddModuleScore was used to compute the normalized weighted mean expression of these genes, and Pearson correlation coefficient was utilized to denote their correlation.

3. Results

3.1. Acquisition of scRNA-seq profiles and identification of single-cell expression atlas of mouse subcutaneous tumors

Experimental workflow was shown in Fig. 1A. The important parameters were exhibited in Table S2. The fitting curve based on the distributions of nGene, nUMI and percent. mito was shown in Fig. S1. The nGene, nUMI and percent. mito per cell before and after QC were displayed in Table S3 and Figs. S2A–B. After QC, 13 clusters were identified, among which cluster 1 was most abundant in αPD-L1 tumor yet cluster 8 and cluster 10 were increased in *Fn* and *Fn* +αPD-L1 tumors (Fig. 1B–C). By calculating the Pearson correlation coefficient of the mean gene expression in each cluster, we found that cluster 1, 2, 3, 4, 5, 6, 7 and 12 had higher correlations with each other than the other cell clusters (Fig. 1D).

To identify cell types, we first mapped the gene expression profile of these cell subsets to the reference dataset of mouse Immgen and then analyzed the well-known markers for common cell types in the TME [21]. It turned out that cluster 8 and cluster 10 had similar expression patterns to monocytes and T cells/NKT cells, respectively (Fig. S3A). Additionally, they had abundant expressions of

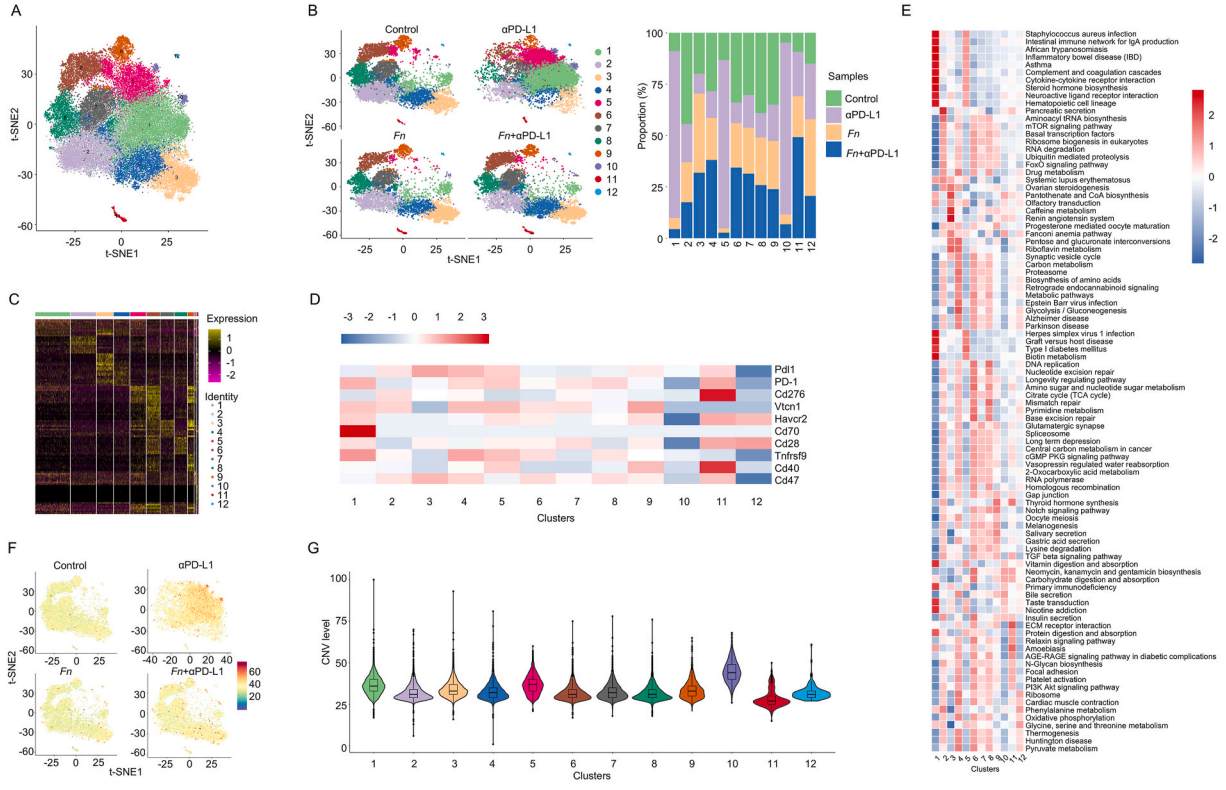

Fig. 2. Tumor cells are divided into 12 subclusters based on differentially expressed genes (DEGs). (A) Tumor cell subclusters in tumor samples. (B) The constitution of cell clusters in different tumor samples and percentages of different tumor samples in the 12 cell subclusters. (C) The top 10 DEGs in each tumor cell subcluster. (D) The expression of several immune checkpoint molecules in each tumor cell subcluster. (E) The Gene Set Variation Analysis (GSVA) results of each tumor cell subcluster. (F) and (G) The CNV level in different tumor samples and tumor cell subclusters, respectively.

monocyte/macrophage markers Cd14/Cd68 and T cell marker Cd3e (Fig. 1E). Therefore, cluster 8 and cluster 10 were initially identified as monocyte derived macrophages and T cells (Fig. 1G). Cluster1-7, cluster 9, cluster 11 and cluster 13 displayed fibroblast gene patterns and highly expressed fibroblast marker molecules Sparc, Dcn and Cald1, while had low levels of epithelial cell marker Epcam, smooth muscle cell marker Smtn and endothelial cell marker Pecam1 (Fig. S3A-B, Fig. 1E) [22–25]. Combined with their higher CNV levels compared with cluster 8 and cluster 10, they were finally considered as tumor cells (Fig. 1F–G, Fig. 3C). Cluster 12 annotated as unknown cells since it expressed both monocyte and fibroblast markers (Fig. 1G).

3.2. Cluster 1 and cluster 5 might be resistant to anti-PD-L1 treatment

To explore the innate and adaptive heterogeneity of tumor cells challenged by different stimulus, we subdivided the malignant cells into 12 subclusters (Fig. 2A). Compared with cell cluster constitution in the control, *Fn* and *Fn*+αPD-L1 samples, tumor cells in αPD-L1 tumor were predominantly enriched in cluster 1, cluster 5 and cluster 10 (Fig. 2B). Since cluster 1 and cluster 5 increased greatly under anti-PD-L1 treatment, there was a suspect that they possibly represented tumor cell populations that were resistant to immunotherapy. Therefore, we subsequently analyzed the differences of genetic characteristics and enriched pathways in the two clusters. According to gene expression characteristics, cluster 1 was named as $Bnip3^{high}Cryab^{high}Hspa1b^{high}$ tumor cells since they had higher expression of autophagy related gene Bnip3, heat shock protein genes Cryab and Hspa1b. Cluster 5 were considered to be a proliferative tumor cell subpopulation based on the levels of Prc1, Cenpf, Mki67, and Fbxo5 expression, which were associated with cell division and proliferation (Fig. 2C and Dataset 1). We further evaluated the expression of common immune checkpoint molecules. It was shown that cluster 1 had remarkably enriched Cd70 while were devoid of Pdl1 expression (Fig. 2D). This partly explained their decreased sensitivity to PD-L1 blockade, and provided an alternative for subsequent ICB therapy when drug resistance occurred.

Next, we conducted GSVA to retrieve the feature for each cluster. The activated and inactivated pathways were identical in cluster 1 and cluster 5 (Fig. 2E). In detail, inflammation associated pathways, such as staphylococcus aureus infection, cytokine receptor interaction and graft versus host disease, were up-regulated. Besides, numerous pathways of DNA replication (DNA replication and homologous recombination), transcription and translation (basal transcription factors, aminoacyl tRNA biosynthesis and ribosome),

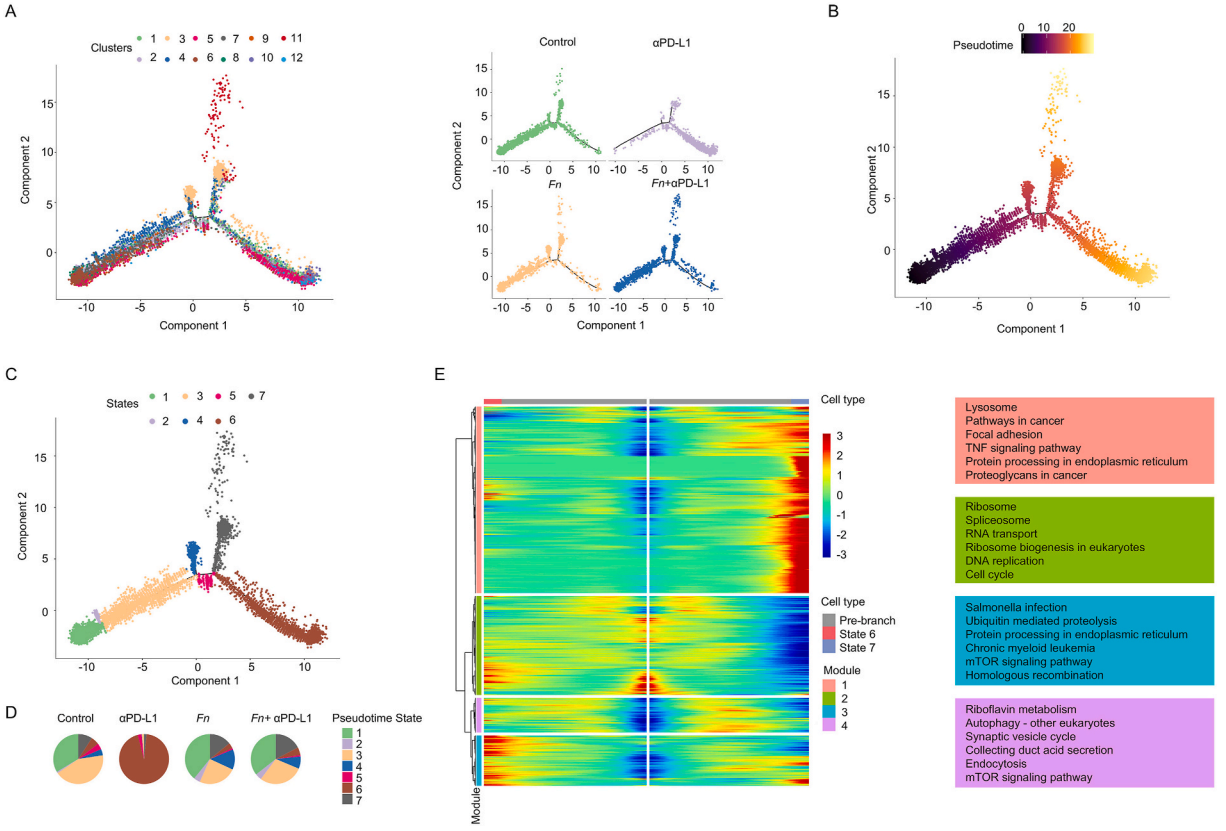

Fig. 3. Pseudotime trajectories of tumor cells are different among distinct tumor microenvironments (TMEs). (A) Pseudotime trajectory of 12 tumor cell subclusters across 4 tumor samples. (B) Pseudotime trajectory according to cell evolution time. The darker the color, the earlier the cells are in the pseudotime differentiation process. (C) Pseudotime analysis of tumor cells based on cell state. (D) The proportions of each cell fate in the 4 tumor samples. (E) Pseudotime heatmap of gene expression and the corresponding enriched pathways. The DEGs along the differentiation trajectory are clustered hierarchically into four modules. The color from blue to red indicates relative expression levels from low to high.

and DNA mismatch repair (nucleotide excision repair and base excision repair) were down-regulated in cluster 1 and cluster 5. In accordance with the dysfunction of DNA mismatch repair, the levels of CNV, or in other words, the somatic copy number aberrations (SCNA) when occurred in tumor cells, were highest in cluster 1, cluster 5 and cluster 10, (Fig. 2F–G). We also found that a series of pathways participating in glycolysis and gluconeogenesis process were downregulated in cluster 1 and cluster 5, such as carbon metabolism, glycolysis/gluconeogenesis, citrate cycle, pyruvate metabolism, oxidative phosphorylation, mTOR signaling pathway and PI3K Akt signaling pathway. By contrast, amino acid metabolism, including phenylalanine metabolism and glycine, serine and threonine metabolism, was up-regulated (Fig. 2E). These results suggested that PD-L1 blockade spurred inflammation, disordered cell cycle, damaged chromosome structure and reprogrammed metabolism style of some tumor cells.

3.3. *Pseudotime trajectory analysis showed distinct differentiation fates of tumor cell subclusters*

As described above, our results revealed that these tumor cell clusters were heterogenous in gene expression profile, implying temporal order of differentiation states during CRC progression. We then pooled all the malignant cells and constructed a single-cell pseudotime trajectory which ordered cells from each cluster and each tumor sample based on their progression states (Fig. 3A). We manually set the root-state of the pseudotime trajectory according to the location of most cells in the control sample (Fig. 3A–B). After calculating the pseudotime value of each cell, they were divided into 7 states (Fig. 3C). Tumor cells originated from state 1, transitioned to state 2, state 3, state 4 and state 5 sequentially, and finally differentiated into two major branches, namely state 6 and 7 (Fig. 3C). It was worth noting that compared with the other three groups, tumor cells of state 6 were predominantly aggregated in anti-PD-L1 treated tumor, while cells in state 7 were similar in percentage among the rest three samples, suggesting that anti-PD-L1 treatment might change the direction of cell differentiation, but this could be reversed by *F. nucleatum* infection (Fig. 3D).

We further illustrated the significantly dynamic gene expression during the evolution into branch state 6 and 7. Gene expression patterns could be classified into 4 modules. Genes of module 1 were up-regulated in state 7 but remained unchanged in state 6. They were enriched in autophagy and metastasis related pathways. In contrast, genes in module 2, participating in cell cycle and DNA replication and repair, were stable in state 6 but down-regulated in state 7. Genes in module 3 had increasing levels in state 6 and were involved in protein metabolism, like ubiquitin mediated proteolysis pathway, protein processing in endoplasmic reticulum, and mTOR signaling pathway. Module 4 contained a group of genes that were upregulated first and but finally returned to relative low levels in both states. The relative pathways contributed to substance metabolism (Fig. 3Eand Dataset 2). These results suggested that immunotherapy and microbiota drove cells to different evolution directions during which process various genes were cooperated to perform specific cellular functions. Thus, understanding their dynamics is important to identify novel treatment targets and reprogram cells towards the less malignant subsets.

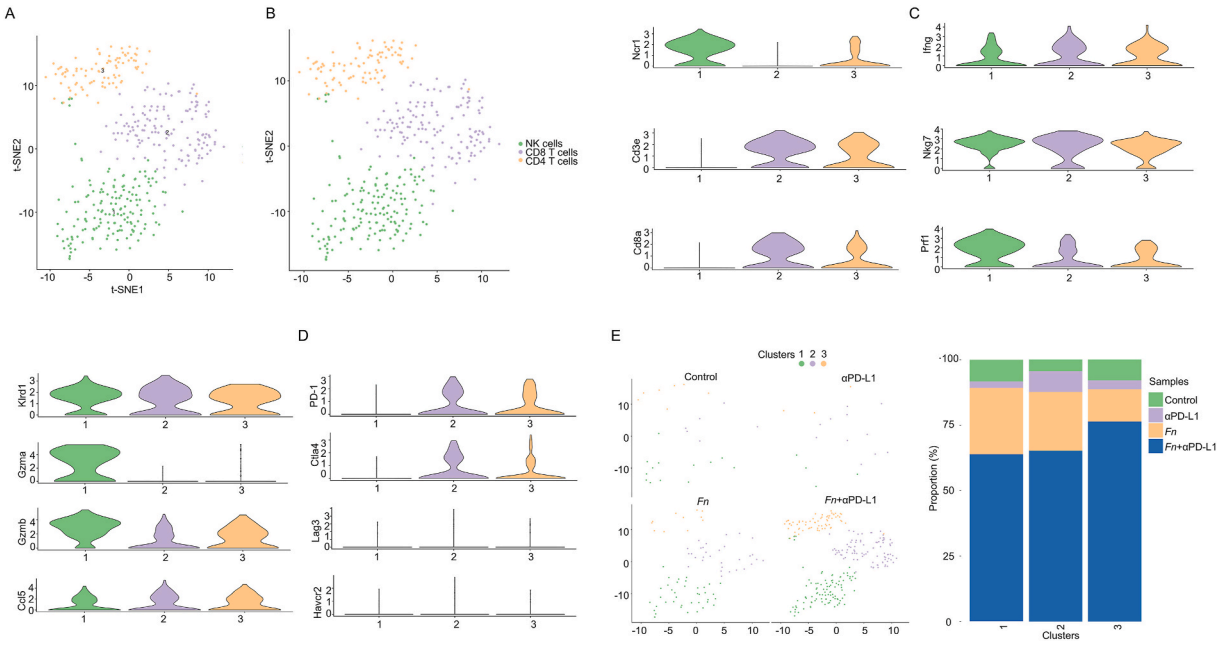

Fig. 4. T cell subcluster richness and gene expression files are influenced by different TMEs. (A) Subclusters of T cells. (B) Cell type identification result. (C) and (D). Cytotoxic molecules and exhausted markers in the 3 clusters. (E) The composition of cell clusters in different tumor samples and the ratio of tumor samples in each of the 3 cell subclusters.

3.4. Enriched effector molecule and low inhibitory molecule expression on NK cells and T cells

Mounting evidence revealed that gut microbiota enriched in CRC shaped immune landscape by modulating the quality and magnitude of immune cells [30,31]. T cell-mediated immune response has a key role in tumor evolution and immunotherapy effect [32]. To address the relationship among *F. nucleatum*, PD-L1 blockade and T cells at scRNA-seq level, we examined the richness and genetic features of T cells in different TMEs.

By t-SNE, T cells were divided into three subclusters (Fig. 4A). As higher expression of Ncr1 was found in cluster 1 while Cd3e and Cd8a were mainly expressed in cluster 2, we characterized cluster 1 as NK cells and cluster 2 as $CD8^+$ T cells. Correspondingly, cluster 3 was identified as $CD4^+$ T cells (Fig. 4B). Exhausted molecules PD-1 and Ctla4 displayed low levels on cluster 2 and cluster 3, while Lag3 and Havcr2 were almost undetectable on all the three clusters (Fig. 4C). In contrast, cytotoxic and effector markers, including Ifng, Nkg7, Prf1, Klrd1, Gzmb and CCL5 were almost ubiquitously expressed in the clusters. In addition, Gzma was enriched in cluster 1 (Fig. 4D). The distributions of cytotoxic molecules in the 3 cell clusters identified them as subsets that mainly exerted anti-tumor effect. By comparing the immune cell richness among different tumor samples, we noticed few T cell infiltration in the control sample and αPD-L1 sample. In contrast, they were increased in *Fn* tumor tissue and more remarkably in *Fn*+αPD-L1 sample (Fig. 4E), suggesting that *F. nucleatum* infection induced effector T cells to the tumor tissue, which could boost immunotherapy efficiency.

3.5. Divergent macrophage subclusters accumulating in Fn and Fn+αPD-L1 tumors

Macrophages are generally categorized into activated pro-inflammatory M1 subtype and alternatively activated M2 subtype with anti-inflammatory role [33]. Despite that *F. nucleatum* resident in the tumor tissue appears to shift macrophage to an M2-like phenotype [34], the abundance and function of these cells might be even more heterogenous.

As above, by performing unsupervised clustering and visualized by t-SNE, we grouped all the collected macrophages from the four tumor samples into 5 subclusters, among which cluster 1 was most abundant (Fig. 5A). Cluster 1, cluster 2 and cluster 3 might be the major cell clusters contributing to immune and inflammatory responses in the TME based on their high functional gene expressions, including Cxcl3, Il1a, Thbs1, Arg1, complement genes (C1qa, C1qb, C1qc), histocompatibility-2 (H2-DMb1, H2-DMb2, H2Aa), Sell, Itga1 and Itga4. Of note, Ly6g was exclusively expressed in cluster 4, thereby this cluster was finally annotated as neutrophils and the rest four subsets as macrophages (Fig. 5B and Dataset 3).

We further conducted macrophage polarization scores and inflammatory scores to have a comprehensive knowledge of the functional characteristics of different cell subclusters based on specific gene sets (Table S1). Phenotypically, cluster 1 had both M1 and M2 features, while the rest of other cell clusters were in unpolarized M0 state, implying the multifunctional roles of tissue-resident macrophages aggregated by *F. nucleatum* (Fig. 5C). When assessing the inflammatory scores, it turned out that the top two

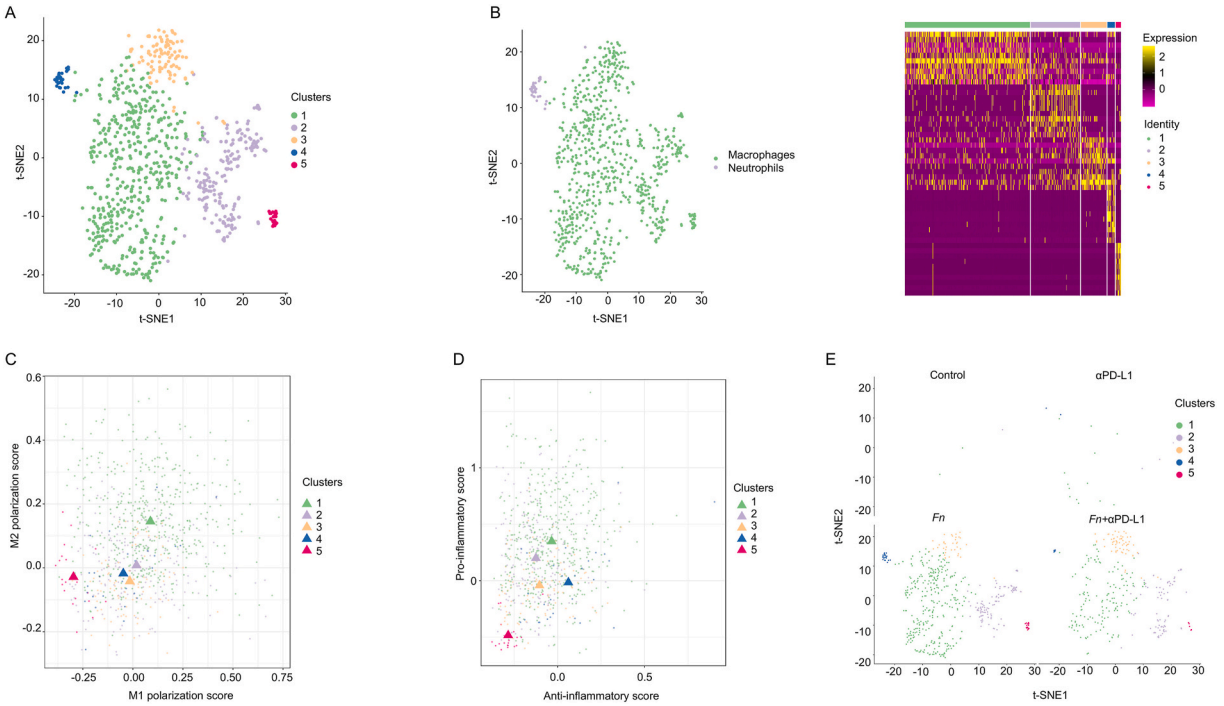

Fig. 5. Macrophage subclusters varied in different TMEs. (A) Subclusters of macrophages. (B) Cell type identification and top 10 DEGs in each cell cluster. (C) Macrophage polarization scores of each subclusters. (D) Inflammatory scores of each macrophage subcluster. (E) The composition of the 5 macrophage subclusters in the four tumor samples.

macrophage clusters, cluster 1 and cluster 2, had positive scores in pro-inflammatory function (Fig. 5D). Finally, we investigated the abundance of macrophage in different TMEs and found that they were more enriched in *Fn*-positive tumor and *Fn*+αPD-L1 sample than αPD-L1 specimen and the control tumor tissue, indicating that the myeloid compartment is also affected by *F. nucleatum* infection (Fig. 5E).

3.6. *F. nucleatum might favor the efficiency of PD-L1 blockade by increasing the cell-cell interactions related to anti-tumor immunity*

As mentioned above, *F. nucleatum* infection influenced the cell composition in the TME, but how it affected cell-cell communication remained to be addressed. Therefore, we compared the interaction number among tumors with distinct treatments using CellChat, which turned out to be higher in *Fn* and *Fn*+αPD-L1 tumors than control and αPD-L1 tumors (Fig. 6A). We then deciphered the specific cell interactions under different TMEs. In the control tumor, we did not detect interactions between macrophages and other cells, and cells in αPD-L1 treated tumor showed no connections with NK cells. Furthermore, T cells sent no signals to tumors after PD-L1 blockade. In contrast, divergent cell types interacted with each other in both the *Fn* and *Fn*+αPD-L1 tumors (Fig. 6B).

We next calculated the difference of molecular interactions before and after anti-PD-L1 mAb treatment in *Fn*-positive and *Fn*-negative tumors respectively to infer the signals which might mediate the enhanced immunotherapy efficiency in *F. nucleatum* colonized carcinoma. Though the recognition between T cells and tumor cells were enhanced indicated by increasing CD8 and MHC-I interactions, no anti-tumor signals were detected in *Fn*-negative tumor after anti-PD-L1 mAb administration. Instead, some tumor promoting connections, especially Spp1 and Fn1 on tumor cells, with their interacting molecules, such as integrins on T cells, as well as Cd44 on macrophages, were enhanced (Fig. 6C) [35–39]. Macrophages and T cells also had crosstalk via Ccl4-Ccr5, Csf1-Csf1r, Cd274-Pdcd1 and Spp1-integrin interactions. Besides, macrophages might have a self-chemotaxis role based on the increasing communications via chemokines and their receptor (Fig. 6C).

In *F. nucleatum* abundant tumor, cell-cell interactions after the addition of anti-PD-L1 mAb differed in striking ways from that of *F. nucleatum*-negative tumor. Among these communications, chemokine-receptor signals pertaining to NK cells were significantly increasing, such as Ccl5-Ccr5, Ccl4-Ccr5, Ccl3-Ccr5 and Ccl2-Ccr2 (Fig. 6D). Since immune system plays a key role in anti-PD-L1 mAb mediated immunotherapy, we paid special attention to anti-cancer signals of the immune cells. It turned out that Ifng-Ifngr1/Ifngr2 interaction between T/NK cells and tumor cells was significantly increased. In addition, T cells and macrophages had enhanced interplay via Cd6-Alcam interaction, which might contribute to the activation, proliferation, and trafficking of T cells, but macrophages also activated Cd86-Ctla4 signal to induce T cell exhaustion [40]. Moreover, tumor cells tried to escape immunosurveillance

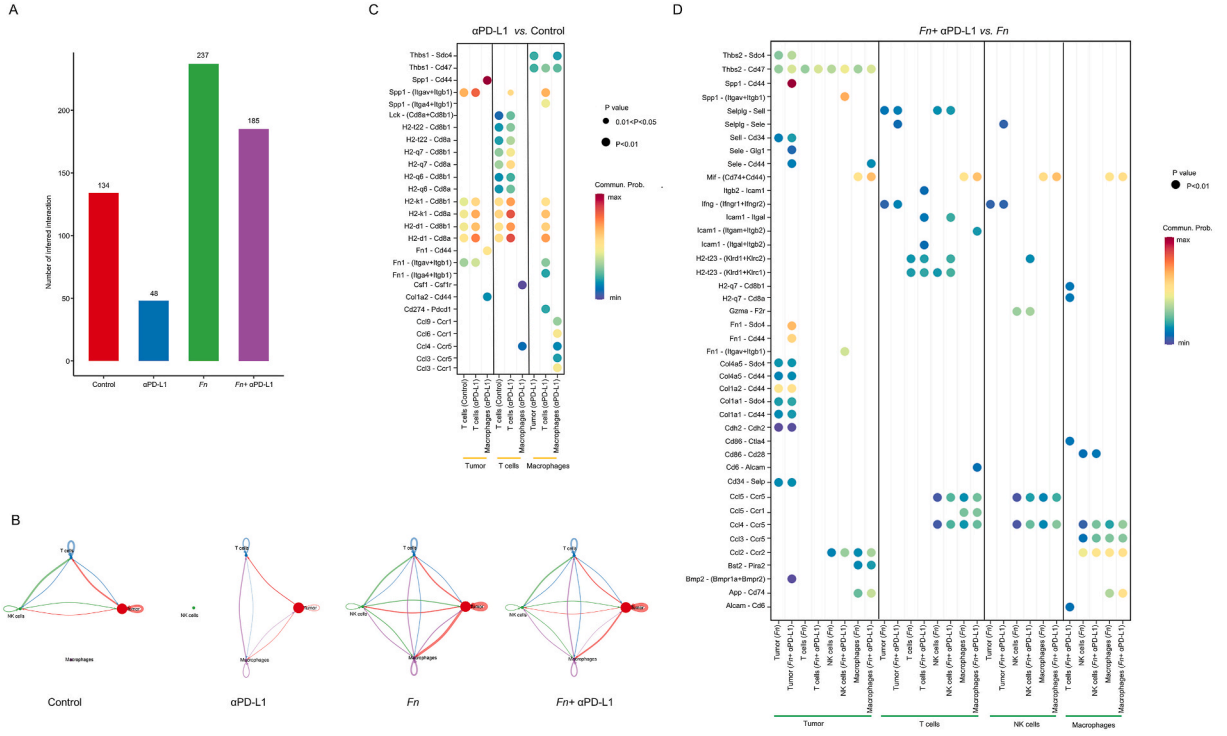

Fig. 6. Cell-cell interactions are more frequent in *Fn*-colonized TMEs. (A) Interaction number of cells in different tumor samples. (B) Cell interaction between different cell types in various TMEs. Arrows indicates the direction of communication. The color suggests cells sending signals. The thickness of lines means communication number. (C) The significantly increasing signaling between different cell types in αPD-L1 treated tumor in contrast to control tumor. (D) The significantly increasing signaling between different cell types in *Fn*+αPD-L1 treated tumor versus *Fn* infected tumor.

through a series of ligand-receptor pair, such as Thbs2-Cd47 between tumor and all three immune cells, Fn1-integrin between tumor and NK cells, and App-Cd47 and Sele-Cd44 between tumor and macrophages, indicating the coexistence of anti-tumor and tumor promoting signals in the TME. Tumor also evolved by increasing autocrine signals, including invasion and migration related signals (Col 4a5-Sdc4/Cd44, Col 1a1-Sdc4/Cd44, Col 1a2-Cd44, Spp1/Fn1-Sdc4/Cd44, Thbs2-Sdc4/Cd47) (Fig. 6D). Collectively, our scRNA-seq data suggested that *F. nucleatum* infection enlivened the TMEs and increased the interaction between divergent cell types, among which the anti-tumor signals might play a critical role in evading tumors.

4. Discussion

Immunotherapy has arouse great excitement owing to its success in achieving long lasting responses in various tumors, including melanoma, lung cancer as well as CRC [10,11,41]. Nevertheless, the dilemma that only a subset of patients is sensitive to this treatment remains a major challenge [17,42]. Therefore, elucidating the underlying mechanisms on immunotherapy resistance contributes to identifying responders and improving efficiency.

In this study, tumor cell clusters exhibited different patterns of immune checkpoint molecules. This explained the unsatisfactory effect of single ICB treatment and hinted alternative or combined targets. Among tumor clusters, Bnip3^{high}Cryab^{high}Hspa1b^{high} cluster 1 and proliferative cluster 5, which thrived dramatically in the anti-PD-L1 treated tumor, were both characterized by DNA repair defects and higher levels of CNV (or called SCNA as in somatic cells). A study on NSCLC patients receiving anti-PD-1/PD-L1 treatment shows that the SCNA is lower in patients with partial response than those with progressive/stable disease, indicating CNV or SCNA as a biomarker for prediction of immunotherapy response [43]. Mechanically, it is considered that highly aneuploid tumors lost genes promoting immune clearance and gained gene escaping from immune surveillance in response to external stress [44,45]. Genomic instability activates cGAS/STING signaling, which has an immediate effect to kill cancer cells by recruiting anti-tumor CD8$^+$ T cells, but eventually results in the failure of immunotherapy due to long-term exposure induced increasing exhausted receptors on T cells [46,47]. Moreover, down-regulated aerobic glycolysis might also lead to insensitivity to anti-PD-L1 treatment in tumor cells, as observed in cluster 1 [48]. Combined with the pseudotime analysis that cells from anti-PD-L1 treated tumor were mainly located at the termination of differentiation, we inferred that immunotherapy pushed certain tumor cell subpopulation to evolve to resistant subclones that failed to boost tumor-specific immunity. Surprisingly, in *F. nucleatum* infected tumors, anti-PD-L1 treatment were unable to cause this transition. Thus, we assumed that *F. nucleatum* enhanced anti-PD-L1 efficiency by switching the fate of tumor cells away from immunotherapy resistant phenotype induced by anti-PD-L1 therapy. But further research is needed to excavate the key molecules involved in this process.

Typically, immune cells play versatile roles in the TME. It has been noted that CD4$^+$ Th1 cells, activated CD8$^+$ T cells, and γδ-T cells often participate in immune responses, whereas Th2, Th17, and Foxp3$^+$ regulatory T cells are often associated with tumor progression [49,50]. Some studies show that B cells could both induce and maintain beneficial antitumor activity and exert protumor functions [51]. Mature and active DCs infiltrated in the tumors induce immune activation and recruit immune effector cells to combat with tumor cells [52]. Myeloid-derived suppressor cells (MDSCs) and tumor-associated macrophages (TAMs) exert potent suppressive activities against effector lymphocytes [53]. Substantial evidence shows that the enhancement of T cell infiltration, particularly the CD8$^+$ T cells, into tumor tissue predicts a superior prognosis and higher responsiveness rate towards ICB [50,54]. *F. nucleatum*-colonized tumor tissues were more enriched in CD8$^+$ T cells and NK cells with high cytotoxic molecule levels compared with *F. nucleatum*-free tissues. Thus we speculated that *F. nucleatum* re-educated the immune-cold TME into immune-hot one to sensitize anti-PD-L1 mAb. Though not plentiful, exhausted biomarker PD-1 was expressed in CD8$^+$ T cell subset. However, this potential tumor-promoting effect of PD1-Pdl1 interaction might be interrupted by anti-PD-L1 treatment. Besides PD-1, Ctla4 was also detected on T cells, which remained us that combined use of Ctla4 blockade and anti-PD-L1 monoclonal antibody could further improve the outcome of patients with *F. nucleatum* colonized CRC.

Macrophages are functionally differentiated into anti-tumoral M1 and pro-tumoral M2 subsets [55–57]. Mounting data has demonstrated that *F. nucleatum* induces macrophages to the tumor sites, which were in consistent with our results [4,58]. Among the macrophages, cluster 1 exhibited both M1 and M2 phenotypes, indicating a versatile role in the TME. The other clusters in M0 state might be targets to improve immunotherapy efficiency by repolarizing macrophages towards the M1 subset secreting anti-proinflammatory cytokines.

Cellular abundance alone does not fully shape the TME. Instead, explicit investigation of cell-cell interactions could provide a better overview. According to our previous study, patients with *Fn*-negative CRC remain resistant to PD-L1 blockade, while *Fn*-positive ones have a higher response rate, indicating that *F. nucleatum* colonized TME benefits immunotherapy [20]. Although subcutaneous tumors with enriched *F. nucleatum* were infiltrated with more lymphocytes as mentioned above, whether and how these cells build connections with tumor cells are not well defined. By interaction analysis, we found increasing interaction number, as well as more complex network in *F. nucleatum* treated tumors versus the control sample, suggesting biological background difference exists, so potential molecular signals mediating improved immunotherapy might be activated in *Fn*-positive tumor tissue after PD-L1 blockade. Exactly, the interferon dependent anti-cancer effect of T cells and NK cells is enhanced in *Fn*-positive tumor. In addition, macrophages also exhibit pro-inflammatory signals, which is consistent with previous report that PD-L1 inhibitor induces macrophage polarizing into more proinflammatory phenotype [59]. More importantly, we speculate that both tumor cells and immune cells potentiates NK cells and macrophages infiltrating into the tumor tissue by strengthening chemokine signals, forming positive feedback to persistently activate anti-tumor immune response. As is known, one of the intrinsic characteristics of tumor cells is to escape immune surveillance [60]. Besides anti-tumor signals, tumor cells also subvert immune cells into immunosuppressive subpopulation via a series of ligand-receptor pairs. Targeting these molecules could ultimately lead to improved immunotherapy or enhanced combination with

anti-PD-L1 therapy. Different from *Fn*-positive tumor, despite that the recognitions are strengthened between T cells and antigen presentation cells dependent on Cd8 and MHC-I interaction, the costimulatory molecules were inhibitory after anti-PD-L1 treatment in *Fn*-negative CRC. Moreover, macrophages in *Fn*-negative TME do not activate pro-inflammatory signals. Thus, for *Fn*-negative tumor, PD-L1 blockade induces immunosuppressive TME instead of boosting effective anti-tumor immune response, which may lead to failure in immunotherapy.

5. Conclusion

According to the current research, only CRC patients with MSI/dMMR could benefit from anti-PD mAb, while patients with MSS/pMMR barely response to this therapy [61]. Therefore, elucidating the mechanisms on immunotherapy resistance is of great significance in identifying efficiency biomarker and targets for combined treatments. In this study, we constructed a subcutaneous colorectal tumor model in mice and used scRNA-seq to explore the comprehensive landscape of CRC. By analyzing the characteristics and interactions of tumor cells, macrophages and T/NK cells in different TMEs, we delineated the composition, subclonal diversity and putative function of distinct cells in the TME, tracked the developmental trajectory of tumor cells and highlighted cell-cell interactions. Thus, we presented a comprehensive insight on the intratumoral heterogeneity of CRC and shed light on the possible mechanisms of immunotherapy resistance from the perspective of tumor cells and immune cells, respectively. Some of our findings has not been reported and need experimental models to validate the speculations. In the further experiment, we plan to build an immunotherapy resistant mice model of CRC, isolate the drug resistant CRC cell and explore their biological characteristics in detail. Besides, how *F. nucleatum* combat with immunotherapy resistance is another interesting topic. By this way, we hope to provide more solutions for overcoming immunotherapy resistance.

Data availability statement

The datasets generated and/or analyzed during the current study are available from the corresponding author on reasonable request.

Ethics statement

The study procedures were approved by the Institutional Animal Care and Use Committee of Shanghai Tenth People's Hospital, School of Medicine, Tongji University (ID Number: SHSY-2018–3566). Animal experiments were conducted in accordance with the National Institutes of Health Guidelines for the Care and Use of Laboratory Animals.

Funding information

This work is supported by the National Natural Science Foundation of China (82273366 and 82072634), Science and Technology Commission of Shanghai (20ZR1442800) and Clinical research plan of SHDC (No. SHDC2020CR2069B and No. SHDC2020CR5006–002).

CRediT authorship contribution statement

Tingting Ding: Writing – original draft, Visualization, Methodology, Formal analysis. **Qian Chen:** Writing – original draft, Visualization, Software, Formal analysis. **Hu Liu:** Software, Methodology, Formal analysis. **Heping Zhang:** Writing – original draft, Software, Methodology. **Yuefang Sun:** Writing – original draft, Software, Methodology. **Lamei Zhao:** Writing – original draft, Software, Methodology. **Yaohui Gao:** Writing – review & editing, Visualization, Validation, Supervision, Project administration, Data curation, Conceptualization. **Qing Wei:** Writing – review & editing, Validation, Supervision, Project administration, Data curation, Conceptualization.

Declaration of competing interest

☒ The authors declare that they have no known competing financial interests or personal relationships that could have appeared to influence the work reported in this paper.

Acknowledgements

We thank OE Biotech Co., Ltd. for their contribution in library construction and sequencing.

Appendix A. Supplementary data

Supplementary data to this article can be found online at https://doi.org/10.1016/j.heliyon.2024.e37511.

References

[1] H. Sung, J. Ferlay, R.L. Siegel, et al., Global cancer statistics 2020: GLOBOCAN estimates of incidence and mortality worldwide for 36 cancers in 185 countries, Ca - Cancer J. Clin. 71 (3) (2021) 209–249, https://doi.org/10.3322/caac.21660.

[2] M. Schmitt, F.R. Greten, The inflammatory pathogenesis of colorectal cancer, Nat. Rev. Immunol. 21 (10) (2021) 653–667, https://doi.org/10.1038/s41577-021-00534-x.

[3] J. Hong, F. Guo, S.Y. Lu, et al., F. nucleatum targets lncRNA ENO1-IT1 to promote glycolysis and oncogenesis in colorectal cancer, Gut 70 (11) (2021) 2123–2137, https://doi.org/10.1136/gutjnl-2020-322780.

[4] C. Xu, L. Fan, Y. Lin, et al., Fusobacterium nucleatum promotes colorectal cancer metastasis through miR-1322/CCL20 axis and M2 polarization, Gut Microb. 13 (1) (2021) 1980347, https://doi.org/10.1080/19490976.2021.1980347.

[5] S. Chen, L. Zhang, M. Li, et al., Fusobacterium nucleatum reduces METTL3-mediated m(6)A modification and contributes to colorectal cancer metastasis, Nat. Commun. 13 (1) (2022) 1248, https://doi.org/10.1038/s41467-022-28913-5.

[6] H.M. Ali, G. Urbinati, M. Raouane, et al., Significance and applications of nanoparticles in siRNA delivery for cancer therapy, Expet Rev. Clin. Pharmacol. 5 (4) (2012) 403–412, https://doi.org/10.1586/ecp.12.33.

[7] G. Urbinati, H.M. Ali, Q. Rousseau, et al., Antineoplastic effects of siRNA against TMPRSS2-ERG junction oncogene in prostate cancer, PLoS One 10 (5) (2015) e0125277, https://doi.org/10.1371/journal.pone.0125277.

[8] G. Urbinati, I. de Waziers, M. Slamic, et al., Knocking down TMPRSS2-ERG fusion oncogene by siRNA could be an alternative treatment to flutamide, Mol. Ther. Nucleic Acids 5 (3) (2016) e301, https://doi.org/10.1038/mtna.2016.16.

[9] H.M. Ali, A. Maksimenko, G. Urbinati, et al., Effects of silencing the RET/PTC1 oncogene in papillary thyroid carcinoma by siRNA-squalene nanoparticles with and without fusogenic companion GALA-cholesterol, Thyroid 24 (2) (2014) 327–338, https://doi.org/10.1089/thy.2012.0544.

[10] A.M.M. Eggermont, C.U. Blank, M. Mandala, et al., Adjuvant pembrolizumab versus placebo in resected stage III melanoma, N. Engl. J. Med. 378 (19) (2018) 1789–1801, https://doi.org/10.1056/NEJMoa1802357.

[11] M. Reck, D. Rodriguez-Abreu, A.G. Robinson, et al., Pembrolizumab versus chemotherapy for PD-L1-positive non-small-cell lung cancer, N. Engl. J. Med. 375 (19) (2016) 1823–1833, https://doi.org/10.1056/NEJMoa1606774.

[12] T. Yau, Y.K. Kang, T.Y. Kim, et al., Efficacy and safety of nivolumab plus ipilimumab in patients with advanced hepatocellular carcinoma previously treated with sorafenib: the CheckMate 040 randomized clinical trial, JAMA Oncol. 6 (11) (2020) e204564, https://doi.org/10.1001/jamaoncol.2020.4564.

[13] R.M. Samstein, C.H. Lee, A.N. Shoushtari, et al., Tumor mutational load predicts survival after immunotherapy across multiple cancer types, Nat. Genet. 51 (2) (2019) 202–206, https://doi.org/10.1038/s41588-018-0312-8.

[14] S.P. Patel, R. Kurzrock, PD-L1 expression as a predictive biomarker in cancer immunotherapy, Mol. Cancer Therapeut. 14 (4) (2015) 847–856, https://doi.org/10.1158/1535-7163.MCT-14-0983.

[15] D.T. Le, J.N. Durham, K.N. Smith, et al., Mismatch repair deficiency predicts response of solid tumors to PD-1 blockade, Science 357 (6349) (2017) 409–413, https://doi.org/10.1126/science.aan6733.

[16] A.M. Luoma, S. Suo, Y. Wang, et al., Tissue-resident memory and circulating T cells are early responders to pre-surgical cancer immunotherapy, Cell 185 (16) (2022) 2918–2935 e2929, https://doi.org/10.1016/j.cell.2022.06.018.

[17] J.S. O'Donnell, G.V. Long, R.A. Scolyer, et al., Resistance to PD1/PDL1 checkpoint inhibition, Cancer Treat Rev. 52 (2017) 71–81, https://doi.org/10.1016/j.ctrv.2016.11.007.

[18] M.D. Vesely, T. Zhang, L. Chen, Resistance mechanisms to anti-PD cancer immunotherapy, Annu. Rev. Immunol. 40 (2022) 45–74, https://doi.org/10.1146/annurev-immunol-070621-030155.

[19] C.B. Zhou, Y.L. Zhou, J.Y. Fang, Gut microbiota in cancer immune response and immunotherapy, Trends Cancer 7 (7) (2021) 647–660, https://doi.org/10.1016/j.trecan.2021.01.010.

[20] Y. Gao, D. Bi, R. Xie, et al., Fusobacterium nucleatum enhances the efficacy of PD-L1 blockade in colorectal cancer, Signal Transduct. Targeted Ther. 6 (1) (2021) 398, https://doi.org/10.1038/s41392-021-00795-x.

[21] T.S. Heng, M.W. Painter, Immunological genome project C, the immunological genome project: networks of gene expression in immune cells, Nat. Immunol. 9 (10) (2008) 1091–1094, https://doi.org/10.1038/ni1008-1091.

[22] Y. Du, X. Jiang, B. Wang, et al., The cancer-associated fibroblasts related gene CALD1 is a prognostic biomarker and correlated with immune infiltration in bladder cancer, Cancer Cell Int. 21 (1) (2021) 283, https://doi.org/10.1186/s12935-021-01896-x.

[23] J.A. Galvan, J. Wiprachtiger, J. Slotta-Huspenina, et al., Immunohistochemical analysis of the expression of cancer-associated fibroblast markers in esophageal cancer with and without neoadjuvant therapy, Virchows Arch. 476 (5) (2020) 725–734, https://doi.org/10.1007/s00428-019-02714-6.

[24] C.F. Guerrero-Juarez, P.H. Dedhia, S. Jin, et al., Single-cell analysis reveals fibroblast heterogeneity and myeloid-derived adipocyte progenitors in murine skin wounds, Nat. Commun. 10 (1) (2019) 650, https://doi.org/10.1038/s41467-018-08247-x.

[25] M. Nurmik, P. Ullmann, F. Rodriguez, et al., In search of definitions: cancer-associated fibroblasts and their markers, Int. J. Cancer 146 (4) (2020) 895–905, https://doi.org/10.1002/ijc.32193.

[26] V. Jelencic, M. Sestan, I. Kavazovic, et al., NK cell receptor NKG2D sets activation threshold for the NCR1 receptor early in NK cell development, Nat. Immunol. 19 (10) (2018) 1083–1092, https://doi.org/10.1038/s41590-018-0209-9.

[27] C. Hermansson, A. Lundqvist, L.U. Magnusson, et al., Macrophage CD14 expression in human carotid plaques is associated with complicated lesions, correlates with thrombosis, and is reduced by angiotensin receptor blocker treatment, Int. Immunopharm. 22 (2) (2014) 318–323, https://doi.org/10.1016/j.intimp.2014.07.009.

[28] E. Vafadarnejad, G. Rizzo, L. Krampert, et al., Dynamics of cardiac neutrophil diversity in murine myocardial infarction, Circ. Res. 127 (9) (2020) e232–e249, https://doi.org/10.1161/CIRCRESAHA.120.317200.

[29] Y. Sun, L. Wu, Y. Zhong, et al., Single-cell landscape of the ecosystem in early-relapse hepatocellular carcinoma, Cell 184 (2) (2021) 404–421 e416, https://doi.org/10.1016/j.cell.2020.11.041.

[30] K. Honda, D.R. Littman, The microbiota in adaptive immune homeostasis and disease, Nature 535 (7610) (2016) 75–84, https://doi.org/10.1038/nature18848.

[31] M. Uribe-Herranz, S. Rafail, S. Beghi, et al., Gut microbiota modulate dendritic cell antigen presentation and radiotherapy-induced antitumor immune response, J. Clin. Invest. 130 (1) (2020) 466–479, https://doi.org/10.1172/JCI124332.

[32] A.D. Waldman, J.M. Fritz, M.J. Lenardo, A guide to cancer immunotherapy: from T cell basic science to clinical practice, Nat. Rev. Immunol. 20 (11) (2020) 651–668, https://doi.org/10.1038/s41577-020-0306-5.

[33] A. Mantovani, A. Sica, Macrophages, innate immunity and cancer: balance, tolerance, and diversity, Curr. Opin. Immunol. 22 (2) (2010) 231–237, https://doi.org/10.1016/j.coi.2010.01.009.

[34] T. Chen, Q. Li, J. Wu, et al., Fusobacterium nucleatum promotes M2 polarization of macrophages in the microenvironment of colorectal tumours via a TLR4-dependent mechanism, Cancer Immunol. Immunother. 67 (10) (2018) 1635–1646, https://doi.org/10.1007/s00262-018-2233-x.

[35] J. Yuan, M. Liu, L. Yang, et al., Acquisition of epithelial-mesenchymal transition phenotype in the tamoxifen-resistant breast cancer cell: a new role for G protein-coupled estrogen receptor in mediating tamoxifen resistance through cancer-associated fibroblast-derived fibronectin and beta1-integrin signaling pathway in tumor cells, Breast Cancer Res. 17 (1) (2015) 69, https://doi.org/10.1186/s13058-015-0579-y.

[36] G. Liu, X. Fan, M. Tang, et al., Osteopontin induces autophagy to promote chemo-resistance in human hepatocellular carcinoma cells, Cancer Lett. 383 (2) (2016) 171–182, https://doi.org/10.1016/j.canlet.2016.09.033.

[37] B. Erdogan, M. Ao, L.M. White, et al., Cancer-associated fibroblasts promote directional cancer cell migration by aligning fibronectin, J. Cell Biol. 216 (11) (2017) 3799–3816, https://doi.org/10.1083/jcb.201704053.

[38] B. Zeng, M. Zhou, H. Wu, et al., SPP1 promotes ovarian cancer progression via Integrin beta1/FAK/AKT signaling pathway, OncoTargets Ther. 11 (2018) 1333–1343, https://doi.org/10.2147/OTT.S154215.

[39] L. Liu, R. Zhang, J. Deng, et al., Construction of TME and Identification of crosstalk between malignant cells and macrophages by SPP1 in hepatocellular carcinoma, Cancer Immunol. Immunother. 71 (1) (2022) 121–136, https://doi.org/10.1007/s00262-021-02967-8.
[40] B. Rambaldi, H.T. Kim, Y. Arihara, et al., Phenotypic and functional characterization of the CD6-ALCAM T-cell co-stimulatory pathway after allogeneic cell transplantation, Haematologica 107 (11) (2022) 2617–2629, https://doi.org/10.3324/haematol.2021.280444.
[41] K. Ganesh, Z.K. Stadler, A. Cercek, et al., Immunotherapy in colorectal cancer: rationale, challenges and potential, Nat. Rev. Gastroenterol. Hepatol. 16 (6) (2019) 361–375, https://doi.org/10.1038/s41575-019-0126-x.
[42] Y. Miao, H. Yang, J. Levorse, et al., Adaptive immune resistance emerges from tumor-initiating stem cells, Cell 177 (5) (2019) 1172–1186 e1114, https://doi.org/10.1016/j.cell.2019.03.025.
[43] H.S. Kim, H. Cha, J. Kim, et al., Genomic scoring to determine clinical benefit of immunotherapy by targeted sequencing, Eur. J. Cancer 120 (2019) 65–74, https://doi.org/10.1016/j.ejca.2019.08.001.
[44] T. Davoli, H. Uno, E.C. Wooten, et al., Tumor aneuploidy correlates with markers of immune evasion and with reduced response to immunotherapy, Science 355 (6322) (2017), https://doi.org/10.1126/science.aaf8399.
[45] M. Chen, R. Linstra, M. van Vugt, Genomic instability, inflammatory signaling and response to cancer immunotherapy, Biochim. Biophys. Acta Rev. Canc 1877 (1) (2022) 188661, https://doi.org/10.1016/j.bbcan.2021.188661.
[46] J.L. Benci, B. Xu, Y. Qiu, et al., Tumor interferon signaling regulates a multigenic resistance program to immune checkpoint blockade, Cell 167 (6) (2016) 1540–1554 e1512, https://doi.org/10.1016/j.cell.2016.11.022.
[47] F. Talens, M. Van Vugt, Inflammatory signaling in genomically instable cancers, Cell Cycle 18 (16) (2019) 1830–1848, https://doi.org/10.1080/15384101.2019.1638192.
[48] D. Guo, Y. Tong, X. Jiang, et al., Aerobic glycolysis promotes tumor immune evasion by hexokinase2-mediated phosphorylation of IkappaBalpha, Cell Metabol. 34 (9) (2022) 1312–1324 e1316, https://doi.org/10.1016/j.cmet.2022.08.002.
[49] K. Okla, D.L. Farber, W. Zou, Tissue-resident memory T cells in tumor immunity and immunotherapy, J. Exp. Med. 218 (4) (2021), https://doi.org/10.1084/jem.20201605.
[50] H. Raskov, A. Orhan, J.P. Christensen, et al., Cytotoxic CD8(+) T cells in cancer and cancer immunotherapy, Br. J. Cancer 124 (2) (2021) 359–367, https://doi.org/10.1038/s41416-020-01048-4.
[51] S.S. Wang, W. Liu, D. Ly, et al., Tumor-infiltrating B cells: their role and application in anti-tumor immunity in lung cancer, Cell. Mol. Immunol. 16 (1) (2019) 6–18, https://doi.org/10.1038/s41423-018-0027-x.
[52] J.M. Tran Janco, P. Lamichhane, L. Karyampudi, et al., Tumor-infiltrating dendritic cells in cancer pathogenesis, J. Immunol. 194 (7) (2015) 2985–2991, https://doi.org/10.4049/jimmunol.1403134.
[53] K. Nakamura, M.J. Smyth, Myeloid immunosuppression and immune checkpoints in the tumor microenvironment, Cell. Mol. Immunol. 17 (1) (2020) 1–12, https://doi.org/10.1038/s41423-019-0306-1.
[54] X. Hu, Y.Q. Li, Q.G. Li, et al., ITGAE defines CD8+ tumor-infiltrating lymphocytes predicting a better prognostic survival in colorectal cancer, EBioMedicine 35 (2018) 178–188, https://doi.org/10.1016/j.ebiom.2018.08.003.
[55] W. Li, X. Zhang, F. Wu, et al., Gastric cancer-derived mesenchymal stromal cells trigger M2 macrophage polarization that promotes metastasis and EMT in gastric cancer, Cell Death Dis. 10 (12) (2019) 918, https://doi.org/10.1038/s41419-019-2131-y.
[56] G.R. Gunassekaran, S.M. Poongkavithai Vadevoo, M.C. Baek, et al., M1 macrophage exosomes engineered to foster M1 polarization and target the IL-4 receptor inhibit tumor growth by reprogramming tumor-associated macrophages into M1-like macrophages, Biomaterials 278 (2021) 121137, https://doi.org/10.1016/j.biomaterials.2021.121137.
[57] G.T. Bardi, M.A. Smith, J.L. Hood, Melanoma exosomes promote mixed M1 and M2 macrophage polarization, Cytokine 105 (2018) 63–72, https://doi.org/10.1016/j.cyto.2018.02.002.
[58] L. Hu, Y. Liu, X. Kong, et al., Fusobacterium nucleatum facilitates M2 macrophage polarization and colorectal carcinoma progression by activating TLR4/NF-kappaB/S100A9 cascade, Front. Immunol. 12 (2021) 658681, https://doi.org/10.3389/fimmu.2021.658681.
[59] H. Xiong, S. Mittman, R. Rodriguez, et al., Anti-PD-L1 treatment results in functional remodeling of the macrophage compartment, Cancer Res. 79 (7) (2019) 1493–1506, https://doi.org/10.1158/0008-5472.CAN-18-3208.
[60] D. Hanahan, R.A. Weinberg, Hallmarks of cancer: the next generation, Cell 144 (5) (2011) 646–674, https://doi.org/10.1016/j.cell.2011.02.013.
[61] D.M. O'Malley, G.M. Bariani, P.A. Cassier, et al., Pembrolizumab in patients with microsatellite instability-high advanced endometrial cancer: results from the KEYNOTE-158 study, J. Clin. Oncol. 40 (7) (2022) 752–761, https://doi.org/10.1200/JCO.21.01874.